

IST-4-027310 MEMBRANE

Deliverable D5.1.2

PHY abstraction methodology and SLS simulator implementation

Contractual Date of Delivery to the CEC:	March 31 st , 2007
Actual Date of Delivery to the CEC:	May 15 th , 2007
Author(s):	A. Maltsev ¹ , V. Sergeyev ¹ , A. Davydov ¹ , A. Maltsev Jr. ¹ , E. Kalantzis ² , A. Valkanas ² , A. Alexiou ³ , F. Boccardi ³ , G Paltenghi ⁴ , K. Leung ⁵ , O. Moreno ⁶
Participants:	INTEL ¹ , ICOM ² , LUCENT ³ , CEFRIEL ⁴ , IMPERIAL ⁵ , TID ⁶
Workpackage:	WP5.1
Est. person months:	20
Security:	Public
Nature:	R
Version:	1.0
Total number of pages:	38

Abstract:

D5.1.2 presents the abstraction model of the MEMBRANE physical layer. Detailed description of the PHY layer abstraction methodology and exact parameters of ready-to-use models are presented. It is shown that single set of parameters of the PHY abstraction model may be used to predict the PHY layer performance of MEMBRANE communication system for different operating scenarios and channels and for various multi-antenna signal processing techniques. Validation of the accuracy of the performance prediction is presented.

Keyword list: Link-level simulations, System-level simulations, PHY abstraction, Multi-antenna techniques, Capacity, Mutual Information

EXECUTIVE SUMMARY

In this report we present the abstraction model of physical (PHY) layer of an OFDMA-based multi-hop communication system. This model is a part of the system level simulation software developed in the work-package WP5.1. The PHY abstraction model is developed for IEEE 802.16e physical layer selected as baseline for MEMBRANE project.

This deliverable describes the PHY abstraction methodology suitable to predict the PHY layer error performance in a realistic channel environment including frequency-selective interference. The approach of predicting the PHY layer performance and the way of obtaining the detailed parameters of PHY abstraction models are presented.

The deliverable also contains detailed parameters of developed PHY abstraction models for several modulation and coding schemes used in the MEMBRANE PHY layer making those models ready to use in system-level simulations for both error performance prediction and for fast link adaptation purposes.

This report also contains results of validation of accuracy of the proposed PHY abstraction methodology. It is shown that the developed PHY abstraction model provides high accuracy of error performance prediction for all MEMBRANE channel models and multi-antenna techniques in both interference and interference-free environments. Therefore the developed PHY abstraction model can serve as a basis for the further system-level simulations.

TABLE OF CONTENTS

EXECUTIVE SUMMARY	2
LIST OF FIGURES	4
LIST OF TABLES.....	6
1 INTRODUCTION	7
2 MEMBRANE PHY LAYER SUMMARY.....	8
2.1 OFDMA Frame structure	8
2.2 PHY layer simulation parameters.....	9
3 PHY ABSTRACTION MODEL	10
3.1 Received signal model.....	10
3.2 Linear MIMO detectors.....	11
3.2.1 Spatial matched detector	11
3.2.2 Zero Forcing detection.....	11
3.2.3 Minimum mean square error (MMSE)	12
3.3 Channel quality indicator – mean instantaneous capacity within FEC block.....	13
3.4 Mutual Information as alternative channel quality indicator.....	13
3.5 Link quality indicator – FEC block error ratio (BLER)	14
4 NUMERICAL PARAMETERS OF PHY ABSTRACTION MODEL	15
4.1 LLS simulation scenarios	15
4.2 MEMBRANE multi-antenna techniques.....	15
4.3 Simulation results	Error! Bookmark not defined.
4.3.1 1 st group of channels	16
4.3.2 2 nd group of channels	19
4.3.3 3 rd group of channels.....	24
4.4 Conclusions on simulation results	27
4.5 Validation of the PHY abstraction methodology.....	28
4.5.1 1 st group of channels	29
4.5.2 2 nd group of channels	30
4.5.3 3 rd group of channels.....	33
4.6 Summary on the PHY abstraction methodology validation	34
5 CONCLUSIONS	35
TERMS AND ACRONYMS.....	36
REFERENCES	38

LIST OF FIGURES

Figure \2.1.1 OFDMA downlink sub-frame illustration.....	8
Figure \2.2.1: Procedure of obtaining the PHY abstraction model.....	10
Figure \3.2.1 : Received BPSK vectors diagram for 2x2 MIMO ZF system in poor conditioned channel for SNR=3 dB.....	12
Figure \4.3.1: PER vs. Capacity scattering diagrams SISO system operating in 1 st group of channels	16
Figure \4.3.2: PER vs. MI scattering diagrams SISO system operating in 1 st group of channels.....	16
Figure \4.3.3: PER vs. Capacity scattering diagrams for 1x4 SIMO system operating in 1 st group of channels..	17
Figure \4.3.4: PER vs. MI Scattering diagrams for 1x4 SIMO system operating in 1 st group of channels	17
Figure \4.3.5: PER vs. Capacity scattering diagrams for 1x4 SIMO system operating in 1 st group of channels in presence of co-channel interference.....	18
Figure \4.3.6: PER vs. MI scattering diagrams for 1x4 SIMO system operating in 1 st group of channels in presence of co-channel interference.....	18
Figure \4.3.7: PER vs. Capacity scattering diagrams for SISO system operating in 2 nd group of channels	19
Figure \4.3.8: PER vs. MI scattering diagrams for SISO system operating in 2 nd group of channels	19
Figure \4.3.9: PER vs. Capacity scattering diagrams for 1x4 SIMO system operating in 2 nd group of channels.	20
Figure \4.3.10: PER vs. MI scattering diagrams for 1x4 SIMO system operating in 2 nd group of channels	20
Figure \4.3.11: PER vs. Capacity scattering diagrams for 1x4 SIMO system operating in 2 nd group of channels in presence of co-channel interference.....	21
Figure \4.3.12: PER vs. MI scattering diagrams for 1x4 SIMO system operating in 2 nd group of channels in presence of co-channel interference.....	21
Figure \4.3.13: PER vs. Capacity scattering diagrams for Alamouti scheme with 2 transmit and 4 receive antennas operating in 2 nd group of channels	22
Figure \4.3.14: PER vs. MI scattering diagrams for Alamouti scheme with 2 transmit and 4 receive antennas operating in 2 nd group of channels	22
Figure \4.3.15: PER vs. Capacity scattering diagrams for Spatial Multiplexing scheme with 2 transmit and 4 receive antennas operating in 2 nd group of channels	23
Figure \4.3.16: PER vs. MI scattering diagrams for Spatial Multiplexing scheme with 2 transmit and 4 receive antennas operating in 2 nd group of channels	23
Figure \4.3.17: PER vs. Capacity scattering diagrams for SISO system operating in 3 rd group of channels	24
Figure \4.3.18: PER vs. MI scattering diagrams for SISO system operating in 3 rd group of channels.....	24
Figure \4.3.19: PER vs. Capacity scattering diagrams for 1x4 SIMO system operating in 3 rd group of channels	25
Figure \4.3.20: PER vs. MI scattering diagrams for 1x4 SIMO system operating in 3 rd group of channels	25
Figure \4.3.21: PER vs. Capacity scattering diagrams for Alamouti scheme with 2 transmit and 4 receive antennas operating in 3 rd group of channels.....	26
Figure \4.3.22: PER vs. MI scattering diagrams for Alamouti scheme with 2 transmit and 4 receive antennas operating in 3 rd group of channels.....	26
Figure \4.5.1: Capacity-based PHY abstraction prediction accuracy for SISO system operating in 1 st group of channels	29

Figure \4.5.2: MI-based PHY abstraction prediction accuracy for SISO system operating in 1 st group of channels	29
Figure \4.5.3: Capacity based PHY abstraction prediction accuracy for 1x4 SIMO system operating in 1 st group of channels	29
Figure \4.5.4: MI based PHY abstraction prediction accuracy for 1x4 SIMO system operating in 1 st group of channels	29
Figure \4.5.5: Capacity based PHY abstraction prediction accuracy for 1x4 SIMO system operating in 1 st group of channels in presence of co-channel interference	30
Figure \4.5.6: MI based PHY abstraction prediction accuracy for 1x4 SIMO system operating in 1 st group of channels in presence of co-channel interference.....	30
Figure \4.5.7: Capacity based PHY abstraction prediction accuracy for SISO system operating in 2 nd group of channels	30
Figure \4.5.8: MI based PHY abstraction prediction accuracy for SISO system operating in 2 nd group of channels	30
Figure \4.5.9: Capacity based PHY abstraction prediction accuracy for 1x4 SMIO system operating in 2 nd group of channels	31
Figure \4.5.10: MI based PHY abstraction prediction accuracy for 1x4 SMIO system operating in 2 nd group of channels	31
Figure \4.5.11: Capacity based PHY abstraction prediction accuracy for 1x4 SMIO system operating in 2 nd group of channels in presence of co-channel interference	31
Figure \4.5.12: MI based PHY abstraction prediction accuracy for 1x4 SMIO system operating in 2 nd group of channels in presence of co-channel interference.....	31
Figure \4.5.13: Capacity based PHY abstraction prediction accuracy for Alamouti scheme with 2 transmit 4 receive antennas operating in 2 nd group of channels.....	32
Figure \4.5.14: MI based PHY abstraction prediction accuracy for Alamouti scheme with 2 transmit 4 receive antennas operating in 2 nd group of channels	32
Figure \4.5.15: Capacity based PHY abstraction prediction accuracy for Spatial Multiplexing scheme with 2 transmit 4 receive antennas operating in 2 nd group of channels	32
Figure \4.5.16: MI based PHY abstraction prediction accuracy for Spatial Multiplexing scheme with 2 transmit 4 receive antennas operating in 2 nd group of channels.....	32
Figure \4.5.17: Capacity based PHY abstraction prediction accuracy for SISO system operating in 3 rd group of channels	33
Figure \4.5.18: MI based PHY abstraction prediction accuracy for SISO system operating in 3 rd group of channels	33
Figure \4.5.19: Capacity based PHY abstraction prediction accuracy for 1x4 SMIO system operating in 3 rd group of channels.....	33
Figure \4.5.20: MI based PHY abstraction prediction accuracy for 1x4 SMIO system operating in 3 rd group of channels	33
Figure \4.5.21: Capacity based PHY abstraction prediction accuracy for Alamouti scheme with 2 transmit 4 receive antennas operating in 3 rd group of channels	34
Figure \4.5.22: MI based PHY abstraction prediction accuracy for Alamouti scheme with 2 transmit 4 receive antennas operating in 3 rd group of channels.....	34

LIST OF TABLES

Table \2.2.1 PHY layer parameters used in LLS simulator	9
Table \4.1.1: representative scenarios for groups of the scenarios	15
Table \4.2.1: list of the most effective multi-antenna techniques for different MEMBRANE scenarios	15
Table \4.3.1: Scattering diagrams and log-linear approximations thereof for SISO system operating in 1 st group of channels	16
Table \4.3.2: Scattering diagrams and log-linear approximations thereof for 1x4 SIMO system operating in 1 st group of channels	17
Table \4.3.3: Scattering diagrams and log-linear approximations thereof for 1x4 SIMO system operating in 1 st group of channels in presence of co-channel interference	18
Table \4.3.4: Scattering diagrams and log-linear approximations thereof for SISO system operating in 2 nd group of channels	19
Table \4.3.5: Scattering diagrams and log-linear approximations thereof for 1x4 SIMO system operating in 2 nd group of channels	20
Table \4.3.6: Scattering diagrams and log-linear approximations thereof for 1x4 SIMO system operating in 2 nd group of channels in presence of co-channel interference	21
Table \4.3.7: Scattering diagrams and log-linear approximations thereof for Alamouti scheme with 2 transmit and 4 receive antennas operating in 2 nd group of channels	22
Table \4.3.8: Scattering diagrams and log-linear approximations thereof for Spatial Multiplexing scheme with 2 transmit and 4 receive antennas operating in 2 nd group of channels	23
Table \4.3.9: Scattering diagrams and log-linear approximations thereof for SISO system operating in 3 rd group of channels	24
Table \4.3.10: Scattering diagrams and log-linear approximations thereof for 1x4 SIMO system operating in 3 rd group of channels	25
Table \4.3.11: Scattering diagrams and log-linear approximations thereof for Alamouti scheme with 2 transmit and 4 receive antennas operating in 3 rd group of channels	26
Table \4.4.1: Parameters of log-linear approximation for PHY abstraction models ($\log_{10}(y)=Ax+B$).....	27

1 INTRODUCTION

The IST Multi-Element Multihop Backhaul Reconfigurable Antenna Network (MEMBRANE) project started in 2006 has the aim to evaluate the applicability of novel multi-hop wireless networks for backhauling data from communication nodes of various types at quality level comparable with one of traditional wired links. To achieve this aim one needs to answer a lot of questions arising from specifics of wireless communication.

Different questions are addressed in different work packages of the MEMBRANE project, and WP 5 is aimed to perform experimental investigations of the performance of the multihop wireless communication system with the help of both computer simulations and proof-of-concept prototyping, and workpackage 5.1 specifically addresses the computer simulations.

Getting representative picture of performance of a communication system as a whole usually requires very extensive computations to take all the factors affecting the system performance such as geographical distribution of nodes, number of antennas and antenna patterns of each node, effectiveness of signal processing algorithms involved, etc into account. To simplify this task simulations may be divided into several stages – first performing measuring performance of single link between two nodes (link-level simulations), then building an abstraction model of the PHY layer based on the results of link-level simulations, and finally measuring the system performance with the help of system-level simulations taking into account geographical parameters of the system deployment, mutual interference, where the performance of each link is obtained from the PHY abstraction model with much less computation efforts than using direct link-level modeling of the PHY layer.

In this deliverable we consider the PHY abstraction model, as an essential part of the System Level Simulator, needed to predict the error performance of the PHY layer using only a small amount of computations. For this purpose a channel quality indicator and a link quality indicator are introduced with the aim to characterize the channel state with as little number of parameters as possible and at the same time allowing prediction of PHY layer error performance with sufficient accuracy.

The deliverable is organized as follows. Section 2 describes OFDMA physical layer specifics that need to be considered when building the PHY abstraction model. The PHY abstraction models are described in detail in Section 3. Section 4 presents the numerical parameters of the MEMBRANE PHY abstraction models and provides the performance evaluation of the models. Conclusions are presented in Section 5.

The material of this deliverable is based on [MEM D21] and [MEM D411], however, the set of the channel models to building the PHY abstraction models for is enlarged as compared to [MEM D411] to align the MEMBRANE simulation platform with the coming multihop wireless standards. The link-level simulator created in the course of [MEM D511] was used to build the PHY abstraction models for typical MEMBRANE scenarios.

2 MEMBRANE PHY LAYER SUMMARY

The PHY layer adopted by the Consortium for the purpose of MEMBRANE link and system-level simulations as well as for the proof-of-concept prototype was IEEE 802.16e OFDMA. Below the features of this physical layer critical for building the PHY abstraction model are described. The OFDMA frame structure is presented to help the reader in understanding of the choice of a channel quality indicators as well as the link quality indicator.

2.1 OFDMA Frame structure

OFDMA data flow is organized as a periodic sequence of data frames, each frame consisting of a downlink (DL) and uplink (UL) subframes split either in time (time-division duplex) or frequency (frequency-division duplex). Below we briefly describe the DL subframe structure.

In frequency domain the OFDM signal is composed of number of orthogonal frequency subcarriers, and in time domain the OFDM signal consists of number of OFDM symbols (see Figure 2.1.1).

First OFDM symbol of an OFDMA DL subframe is the OFDMA preamble. The preamble is chosen from a set of predetermined signals and is used for frame detection, synchronization, channel estimation and other acquisition purposes as well as for distinguishing between the Base Stations because each Base station is assigned a particular preamble from the set thereof.

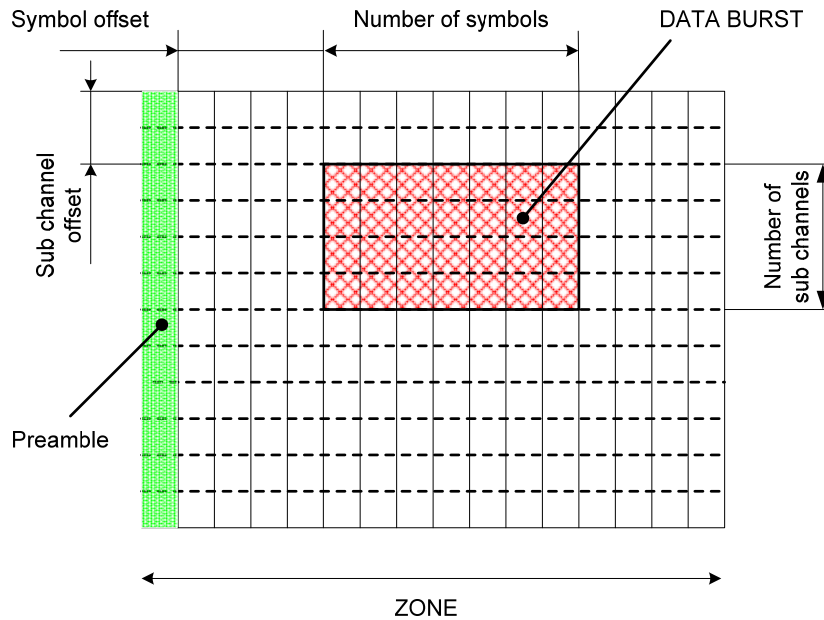


Figure 2.1.1 OFDMA downlink sub-frame illustration

The OFDMA preamble is followed by a data-transmission part of DL subframe. The data transmissions are organized in the following way. The subcarriers are grouped into number of *OFDMA subchannels*, and the OFDM symbols grouped into number of *symbol-slots*. A time-frequency unit having dimensions of one subchannel in frequency and one symbol-slot in time is called an *OFDMA slot*.

During the modulation process, the data are split into *FEC blocks* of predetermined size, each FEC block being independently encoded by the FEC coder at the transmitter and independently decoded at the receiver. After the mapping of the encoded bits to QPSK or QAM symbols, the FEC block occupies one or more OFDMA slots. The largest FEC block corresponding to the QPSK modulation and code rate $\frac{1}{2}$ occupy 10 OFDMA slots under PUSC permutation (defined below).

Several subcarriers of each subchannel are *pilot* subcarriers that carry predetermined signals and may be used for purposes of channel estimation and tracking and timing synchronization maintenance.

Data are transmitted in rectangular areas having dimensions of several slots in frequency by several slots in time. Such an area is called a *data burst* or simply a *burst*. Each burst may be addressed to particular subscriber or a group thereof. Special *DL_MAP* message is provided at the beginning of each DL subframe to signal the burst displacement and dimensions to remote stations. Similar message named *UL_MAP* may be provided after the *DL_MAP* to signal displacement of data bursts in uplink subframe.

The way the subcarriers are grouped into the subchannels and OFDM symbols into symbol-slots can vary within one DL subframe. Areas in the DL subframe having constant structure of subchannels and symbol-slots are called a *zone*. Zones are divided in time domain only and no burst spans over more than one zone.

The way the subcarriers are grouped into the subchannels is defined by a *permutation*. There are four permutations defined for downlink, namely PUSC (stands for partial usage of subchannels), FUSC (full usage of subchannels), TUSC (tile usage of subchannels) and AMC (adaptive modulation and coding).

The first three permutations are distributed permutations. This means that subcarriers of a subchannel are distributed over the entire frequency bandwidth of the channel to increase frequency diversity. For example, under PUSC permutation the subchannel consists of subcarriers quasi-randomly chosen from the whole set thereof. Unlike this, under AMC permutation the subcarriers of a subchannel are adjacent in frequency. Although adjacent permutation has less frequency diversity, it allows for using various adaptive techniques such as adaptive selection of modulation and coding schemes, adaptive assignment of subchannels for users and the like.

2.2 PHY layer simulation parameters

Table 2.2.1 summarizes the PHY layer parameters used to generate the PHY abstraction models of this Deliverable. In order to allow performing validation of the developed PHY abstraction methodology these parameters are set the same as in link level simulations of the [MEM D511]. This allows comparing the PER performance predicted with the help of PHY abstraction models with one directly measured in [MEM D511].

Table 2.2.1 PHY layer parameters used in LLS simulator

Parameter name	Value	Units
Channel frequency bandwidth	10(*)	MHz
Number of subcarriers	1024	
Minimal sampling frequency	11.424	MHz
OFDM Symbol duration	89.6	us
Cyclic prefix duration	1/8	OFDM symbol duration
OFDM Symbol duration with CP	100.84	us
Error-correcting codes	Tail-biting Convolutional, Convolutional Turbo	
Permutation schemes	PUSC, FUSC, AMC	

(*) The bandwidth of the MEMBRANE communication system may occupy up to 100 MHz in 10 MHz increments, however, to reduce the computational efforts LLS simulations consider only 10 MHz channel bandwidth. Such a simplification will not affect the accuracy of future deliverables namely D5.1.2 considering PHY layer abstraction and D 5.1.3 concerning the system-level simulations as the simulation results obtained in this work-package are easily scalable for the desired channel bandwidth.

3 PHY ABSTRACTION MODEL

The PHY abstraction model is the essential block for the system level simulations. The purpose of the PHY abstraction model is to describe a procedure of accurate estimation of the link performance (e.g., BER, PER) of each network node for known block length, selected PHY transmission mode, scheduling decisions, resource allocation, propagation conditions, and inter-cell interference, without really performing the complete link level signal processing. It is desirable that the modeling captures transceiver characteristics, including, e.g., transmitter and receiver signal processing algorithms.

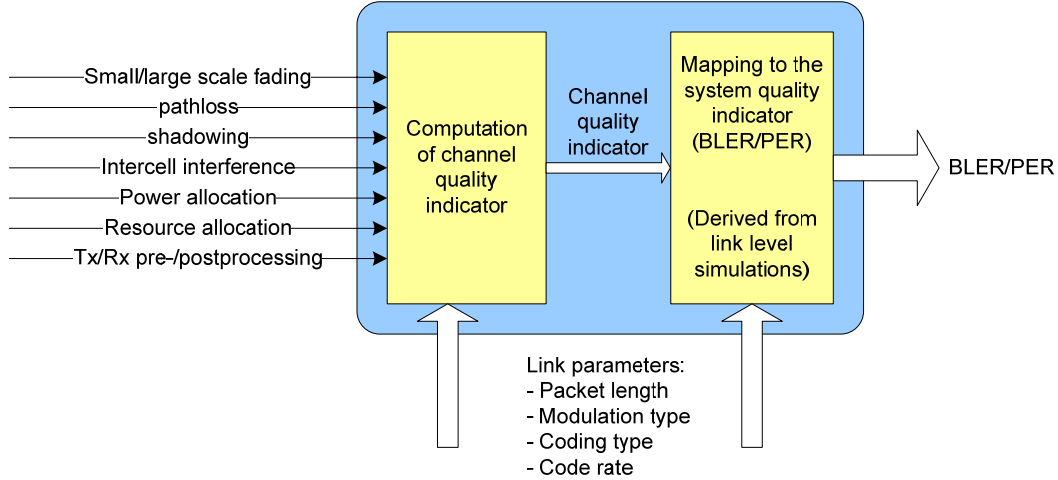


Figure 2.2.1: Procedure of obtaining the PHY abstraction model

PHY abstraction model provides an estimate of the link performance (e.g., PER) when decisions on the RRM, scheduling, and link adaptation are already known. It generates bit or block error probabilities and is utilized for estimation of the quality of the signal reception at run-time, which in turn can generate, for example, re-transmissions and affect also slow link adaptation, such as outer loop power control. The PHY abstraction model may be viewed as a conditional probability; the probability that the transmitted code word is decoded erroneously given the channel, Tx power, beam forming weights, and interference plus noise during the transmission of a data block.

3.1 Received signal model

Consider OFDMA system employing multiple antennas at both sides. In case of ISI-free channels and perfect channel estimation and synchronization, the per-subcarrier received signal model can be written as follows:

$$\mathbf{y}_p = \mathbf{H}_p \cdot \mathbf{s}_p + \sum_{k=1}^{N_{BS}} \mathbf{G}_p^{(k)} \cdot \mathbf{x}_p^{(k)} + \mathbf{n}_p \quad 3.1.1$$

where \mathbf{y}_p is the received signal vector at p^{th} subcarrier, \mathbf{s}_p is the transmitted signal vector, \mathbf{H}_p is the channel matrix of serving station, $\mathbf{G}_p^{(k)}$ is the channel matrix of k^{th} interfering station, $\mathbf{x}_p^{(k)}$ is the transmitted symbol vector from k^{th} interfering station, \mathbf{n}_p - Additive White Gaussian Noise (AWGN) vector. The instantaneous interference-plus-noise correlation matrix can be written as

$$\mathbf{R}_p = \sum_{k=1}^{N_{BS}} (\mathbf{G}_p^{(k)} \cdot \mathbf{G}_p^{(k)H}) \cdot B_p^{(k)} \cdot \text{hit}_p^{(k)} + \sigma_n^2 \mathbf{I} \quad 3.1.2$$

where N_{BS} is the number of interfering stations, $B_p^{(k)}$ - power boosting coefficient, $hit_p^{(k)}$ - subcarrier hit indicator (1 if the transmitting node and k^{th} interfering node are both using the p^{th} subcarriers and 0 otherwise) and σ_n^2 - is a power of AWGN.

In the following discussion all receivers depending on interference knowledge can be classified in two types:

- matched or interference-aware receivers and,
- mismatched or interference-agnostic receivers

The difference between the two receivers is in the assumptions they make about the structure of noise and interference. While matched receivers use full information about the interference (which can be obtained from per-subcarrier estimation of interference-noise correlation matrix), interference-agnostic receivers rely on the AWGN assumption of additive interference-noise which is mathematically expressed by setting $\mathbf{R}_p = \mathbf{I}$ in the following equations. This assumption may be good as long as there are many interfering stations operating in the same channel, however for limited number of interferers, such an assumption may lead to performance degradation of the system due to non-optimal signal demodulation/decoding.

It should be noted that the PHY layer abstraction models presented in this report are built for the interference-aware receiver.

3.2 Linear MIMO detectors

Assuming channels with additive Gaussian noise the optimal maximum-likelihood detector (MLD) will estimate the transmitted signal vector \mathbf{s}_p by minimizing the norm:

$$\hat{\mathbf{s}}_p = \arg \min_{\mathbf{x}_p} (\mathbf{y}_p - \mathbf{H}_p \mathbf{s}_p)^H \mathbf{R}_p^{-1} (\mathbf{y}_p - \mathbf{H}_p \mathbf{s}_p) \quad 3.2.1)$$

In case of direct search over all possible combinations of vector \mathbf{s}_p the ML detection requires large amount of hypothesis to test. This makes MLD approach prohibitive for implementation especially in case of big constellations and large number of parallel spatial streams. Therefore, below we consider linear MIMO detectors like spatial matched detector (SMD), zero-forcing (ZF) and minimum mean square error (MMSE), which may provide the performance close to optimal at the significantly reduced implementation complexity.

3.2.1 Spatial matched detector

One of the conventional approaches for demodulation of the received signal is Spatial Matched Detector (SMD) that may be described by a linear operator

$$\mathbf{P}_p^{\text{MF}} = \mathbf{H}_p^H \mathbf{R}_p^{-1} \quad 3.2.2)$$

which is applied to the received signal vector. This detector basically maximizes the output Signal-to-Noise Ratio (SNR). Unfortunately, in the case of transmission of multiple spatial streams the SMD does not cancel mutual interference between the streams. The most typical application of this detector is demodulation of STC-‘A’ codes in noise-limited scenarios. It was shown in [Alamouti] that SMD provides maximum-likelihood demodulation (with slicing or LLR extraction and channel decoding) of transmitted signal vector $\mathbf{s}_p = (s_1 \ s_2)^T$ in quasi-static channels.

3.2.2 Zero Forcing detection

In contrast to SMD, Zero Forcing (ZF) detection perfectly suppresses mutual interference between the spatial streams. ZF detection is accomplished by applying Moore-Penrose pseudo-inverse operator to the received signal:

$$\mathbf{P}_p^{\text{ZF}} = (\mathbf{H}_p^H \mathbf{R}_p^{-1} \mathbf{H}_p)^{-1} \cdot \mathbf{H}_p^H \mathbf{R}_p^{-1} \quad 3.2.3)$$

It can be shown that the output noise from ZF detector is spatially correlated and has a covariance matrix equal to $(\mathbf{H}_p^H \mathbf{R}_p^{-1} \mathbf{H}_p)^{-1}$. Therefore poorly conditioned channel with small eigenvalues of matrix $\mathbf{H}_p^H \mathbf{R}_p^{-1} \mathbf{H}_p$ can result in significant noise amplification in the directions of corresponding eigenvectors. This is illustrated in Figure 3.2.1 for MIMO system with two spatial streams and BPSK modulations in both channels. In this figure the output vector elements from ZF detector are depicted along horizontal and vertical axes, and red lines show the hard decision boundaries for BPSK modulation.

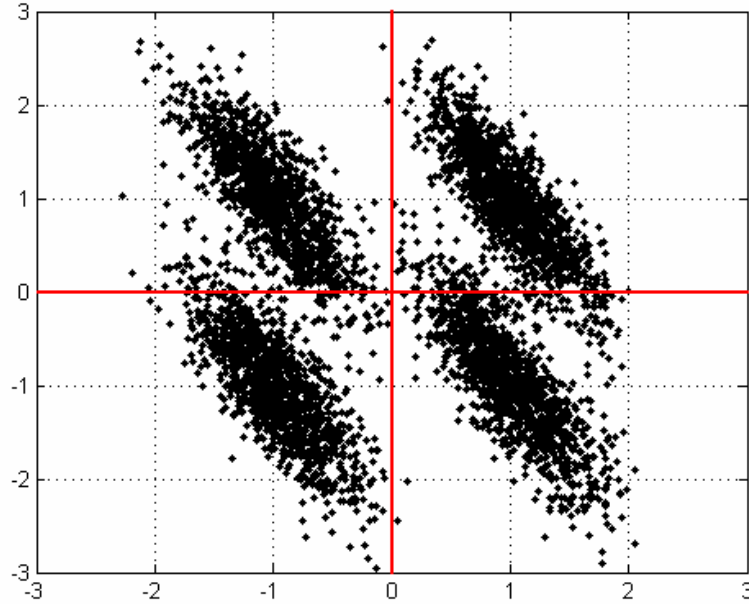


Figure 3.2.1 : Received BPSK vectors diagram for 2x2 MIMO ZF system in poor conditioned channel for SNR=3 dB

3.2.3 Minimum mean square error (MMSE)

A better receiver is the Minimum Mean Square Error (MMSE) receiver that performs weighted inverse of the channel matrix so as to keep the balance between cancellation of interference *from other spatial streams* and noise amplification. The MMSE solution minimizes the total error (MSE) including noise and interference from other spatial streams, i.e.

$$\mathbf{P}_p^{\text{MMSE}} = \arg \min_{\mathbf{P}_p} E(\|\mathbf{x}_p - \mathbf{P}_p \mathbf{s}_p\|^2) \quad (3.2.4)$$

MMSE solution can be expressed by the linear operator:

$$\mathbf{P}_p^{\text{MMSE}} = (\mathbf{H}_p^H \mathbf{R}_p^{-1} \mathbf{H}_p + \mathbf{I})^{-1} \mathbf{H}_p^H \mathbf{R}_p^{-1} \quad (3.2.5)$$

Mean square error for k^{th} spatial stream at the output of MMSE detector is equal to

$$\text{MSE}_k = (\mathbf{H}_p^H \mathbf{R}_p^{-1} \mathbf{H}_p + \mathbf{I})_{k,k}^{-1} \quad (3.2.6)$$

It can be verified that MMSE estimation is biased, and relative bias for k^{th} spatial stream is

$$\beta_k = 1 - \frac{1}{\text{SINR}_k} \quad (3.2.7)$$

where SINR_k is Signal-to-Interference-plus-Noise ratio for k^{th} output of MMSE detector. It can be shown that after bias removing the unbiased Signal-to-Interference-Noise ratio will be equal to

$$\text{SINR}_k^{\text{unbiased}} = \text{SINR}_k - 1 \quad (3.2.8)$$

In our simulations we use the actual unbiased $\text{SINR}_k^{\text{unbiased}}$ for k^{th} spatial stream for scaling LLR values from the demapper output.

It is interesting to consider the asymptotic behavior of MMSE detector in high and low SNR ranges. In the case of low SNR, MMSE solution is converging to spatial matched detection: $\mathbf{P}_p^{\text{MMSE}} \rightarrow \mathbf{P}_p^{\text{MF}} = \mathbf{H}_p^H \mathbf{R}_p^{-1}$. The spatial matched detector optimally combines received signals and reduces noise, but does not eliminate interferences from neighboring spatial streams. In the case of high SNR, the MMSE detection gives Zero-Forcing solution, which perfectly decouples received signals into several independent spatial streams: $\mathbf{P}_p^{\text{MMSE}} \rightarrow \mathbf{P}_p^{\text{ZF}} = (\mathbf{H}_p^H \mathbf{R}_p^{-1} \mathbf{H}_p)^{-1} \mathbf{H}_p^H \mathbf{R}_p^{-1}$. The MMSE MIMO detector is used in the receive signal processing in the MEMBRANE nodes. Therefore the PHY abstraction models are also built for the MMSE receiver.

3.3 Channel quality indicator – mean instantaneous capacity within FEC block

The calculation procedure for mean instantaneous capacity within a FEC block is as follows. First one needs to calculate the SINR values for each subcarrier and then calculate the capacity of each subcarrier using the classical formula:

$$c(k) = \log_2(1 + \gamma_{pp}(k)) \quad (3.3.1)$$

where $\gamma_{pp}(k)$ is instantaneous post-processing SINR value for k^{th} subcarrier. Post-processing here means SINR after applying multi-antenna processing and removing spatial diversity. To obtain mean capacity within the FEC block one needs to determine the set of subcarriers the FEC block is mapped to and average the capacity value over this set of subcarriers:

$$C_m = \frac{1}{N} \sum_{k=1}^N c(k) \quad (3.3.2)$$

Using mean instantaneous capacity within the FEC block as channel quality indicator has an advantage of being simple to calculate from the vector of subcarrier SINR. This saves the simulation time during system-level performance evaluation.

3.4 Mutual Information as alternative channel quality indicator

Recent research [Ericsson], [Caire] indicates that mutual information (MI) can be used as channel quality indicator providing high accuracy of prediction PHY layer performance. The mutual information for i^{th} subcarrier is computed as a function of the M-ary modulation scheme, with m bits/symbol, as follows:

$$MI(\text{SINR}(i), m(i)) = E_{XY} \left(\log_2 \left(\frac{P(Y | X, \text{SINR}(i))}{\sum_X P(X) P(Y | X, \text{SINR}(i))} \right) \right) \quad (3.4.1)$$

In the above, Y is the received symbol and $P(Y | X, \text{SINR})$ is the AWGN channel transition probability density conditioned on the input symbol X. It is assumed that $P(X) = 1/M$, where M is the size of the M-ary modulation alphabet.

Assuming N sub-carriers are used to transmit a coded block, the received mutual information over a coded block is computed as:

$$RBI(i) = \sum_{i=1}^N MI(SINR(i), m(i)) \quad (3.4.2)$$

We note that the even though we refer to the coded block being carried over a set of sub-carriers, in general, the coded block may be carried over multiple dimensions, including the spatial dimensions available with MIMO.

3.5 Link quality indicator – FEC block error ratio (BLER)

A link quality indicator is the measure of error performance of the link. The whole range of characteristics may be proposed for use as a candidate link quality indicator, for example, bit error rate (BER), OFDMA slot error rate (SLER), packet error rate (PER), or some other measures. Typical error performance measure is PER, however, using it as a link quality indicator is not convenient because PER depends not only on the channel state, but also on the size of the packet, which is hard to predict especially in the case of using packet segmentation and adaptive scheduling. BER is not convenient either because complicated forward error correction (FEC) coding schemes do not allow simple calculation of PER from it.

For OFDMA PHY the much more flexible and convenient performance measure is the error ratio of OFDMA FEC coding blocks (BLER) for several of reasons. As it is described in [802.16] an OFDMA data burst may consist of one or more FEC coding blocks, each block being encoded and decoded independently. The FEC block may be considered as a minimal independent “brick” which packets (bursts) are constructed from. The size of FEC blocks is up to 60 bytes, and therefore it is very likely that a typical burst contains more than one FEC block. Since FEC blocks are encoded and decoded independently, knowing the BLER it is simple to predict error ratios of bursts of any size using the formula:

$$PER = 1 - (1 - BLER)^N, \quad (3.5.1)$$

where PER is error probability of a burst, N is the number of FEC blocks in the burst.

It should be noted that for low order modulation such as QPSK at code rate $\frac{1}{2}$ a FEC block may occupy up to ten OFDMA slots and therefore it is possible for the FEC block to have various dimensions in terms of number of subcarriers and number of OFDMA symbols. This adds some uncertainty in the sense that FEC blocks of the same size in bytes in the same channel at the same SINR may have different error ratios depending on their dimensions. However, for PUSC permutation performing quasi-random reordering of the subcarriers this effect is not substantial. On the other hand for higher-order modulation and coding schemes FEC blocks occupy fewer OFDMA slots thus further reducing this uncertainty.

4 PARAMETERS OF THE PHY ABSTRACTION MODEL

4.1 MEMBRANE scenarios used to obtain the PHY abstraction models

In [MEM D511] it was shown that all MEMBRANE link-level channel models may be subdivided into three groups characterized with distinct system behaviour therein. For channel models within one group the error performance depending on SNR does not vary considerably. On the other hand the aim of this deliverable is to develop PHY abstraction model which is not sensitive to the channel type used. Therefore to prove the robustness of the developed PHY abstraction model to the channel type, it is sufficient to simulate and compare the accuracy of PHY error performance prediction in channels of different groups. For generating of parameters and performance validation of the PHY abstraction model we have used the following MEMBRANE scenarios with associated channel models as typical representatives of the channel groups:

Table 4.1.1: representative scenarios for groups of the scenarios

Groups of channels	1 st group	2 nd group	3 rd group
Representative scenario	U2a LOS	U2c LOS	R1 NLOS

4.2 MEMBRANE multi-antenna techniques

Besides the representative MEMBRANE scenarios the deliverable [MEM D511] has also identified the most effective and useful techniques for each group of MEMBRANE scenarios and showed that certain multi-antenna techniques have little or no effect in certain groups of channels. Therefore ineffective techniques will be excluded from further investigation to reduce the amount of computational efforts if future workpackages. The following multi-antenna techniques will be investigated with respect to particular MEMBRANE groups of channels:

Table 4.2.1: list of the most effective multi-antenna techniques for different MEMBRANE scenarios

	1 st group	2 nd group	3 rd group
Multi-antenna techniques	SISO SIMO (1x4)	SISO SIMO (1x4) STC-A (Alamouti code, 2x4) STC-B (spatial multiplexing, 2x4)	SISO SIMO (1x4) STC-A (Alamouti code, 2x4)

4.3 Numerical parameters of the PHY abstraction model

In the paragraphs below the simulation results are presented in the following format. For each group of channels and for each simulated multi-antenna technique a figure illustrating the scattering diagrams in CQI-PER axes as well as log-linear approximation of the results is presented. In figures the PER (packet error rate) was measured for the packet size equal to one FEC block so that figures represent the FEC block error ratio vs. the CQI. Four modulation and coding schemes out of all possible are illustrated: QPSK $\frac{1}{2}$, QAM16 $\frac{1}{2}$, QAM64 $\frac{1}{2}$ and QAM64 $\frac{5}{6}$.

Each figure is provided with the log-linear approximation parameters for each simulated modulation and coding scheme.

4.3.1 1st group of channels

4.3.1.1 SISO

Table 4.3.1: Scattering diagrams and log-linear approximations thereof for SISO system operating in 1st group of channels

	<p>Parameters of log-linear approximation ($\log_{10}(y)=Ax+B$):</p> <p>QPSK 1/2: A=-7.9425, B=9.1066</p> <p>QAM16 1/2: A=-5.9373, B=14.1376</p> <p>QAM64 1/2: A=-3.7537, B=13.6966</p> <p>QAM64 5/6: A=-2.9254, B=16.3931</p>
	<p>QPSK 1/2: A=-10.8459, B=11.9316</p> <p>QAM16 1/2: A=-6.5685, B=14.6489</p> <p>QAM64 1/2: A=-3.8171, B=12.8048</p> <p>QAM64 5/6: A=-4.4416, B=22.8895</p>

For SISO system operating in the first group of channels the falloffs of the scattering diagrams are well approximated with log-linear dependence for both Capacity and MI channel quality indicators (CQI). This remains true even for high-order modulations (e.g. QAM64 with code rate 5/6). Small deviation of the points of scattering diagram from approximating curve allows expecting high accuracy of the PHY layer performance prediction in this channel using either of the CQIs.

4.3.1.2 SIMO 1x4 with MRC at the receiver

Table 4.3.2: Scattering diagrams and log-linear approximations thereof for 1x4 SIMO system operating in 1st group of channels

	<p>Parameters of log-linear approximation ($\log_{10}(y)=Ax+B$):</p> <p>QPSK 1/2: $A=-8.8776$, $B=10.1673$</p> <p>QAM16 1/2: $A=-5.5431$, $B=13.0476$</p> <p>QAM64 1/2: $A=-3.9074$, $B=14.2698$</p> <p>QAM64 5/6: $A=-3.0003$, $B=16.7248$</p>
<p>Figure 4.3.3: PER vs. Capacity scattering diagrams for 1x4 SIMO system operating in 1st group of channels</p>	<p>QPSK 1/2: $A=-10.5905$, $B=11.6466$</p> <p>QAM16 1/2: $A=-5.8983$, $B=13.0051$</p> <p>QAM64 1/2: $A=-4.0206$, $B=13.519$</p> <p>QAM64 5/6: $A=-4.233$, $B=21.7747$</p>
	<p>QPSK 1/2: $A=-10.5905$, $B=11.6466$</p> <p>QAM16 1/2: $A=-5.8983$, $B=13.0051$</p> <p>QAM64 1/2: $A=-4.0206$, $B=13.519$</p> <p>QAM64 5/6: $A=-4.233$, $B=21.7747$</p>
<p>Figure 4.3.4: PER vs. MI Scattering diagrams for 1x4 SIMO system operating in 1st group of channels</p>	

It can be seen that for SIMO system with 1 Tx and 4 Rx antennas operating in the first group of channels the falloffs of the scattering diagrams are well approximated with log-linear dependence for both Capacity and MI CQIs. The deviation of the points of scattering diagrams from approximating curves is even smaller than for SISO system operating in the same channel. Comparing PHY abstraction model parameters of each modulation and coding scheme, one can note that they are similar for SIMO and SISO systems.

4.3.1.3 SIMO 1x4 with MMSE receiver in presence of co-channel interference

Table 4.3.3: Scattering diagrams and log-linear approximations thereof for 1x4 SIMO system operating in 1st group of channels in presence of co-channel interference

	<p>Parameters of log-linear approximation ($\log_{10}(y)=Ax+B$):</p> <p>QPSK 1/2: A=-9.5222, B=10.9569</p> <p>QAM16 1/2: A=-5.0531, B=11.8297</p> <p>QAM64 1/2: A=-3.6666, B=13.3492</p> <p>QAM64 5/6: A=-3.0271, B=16.9112</p>
	<p>QPSK 1/2: A=-11.3765, B=12.563</p> <p>QAM16 1/2: A=-5.3988, B=11.8422</p> <p>QAM64 1/2: A=-3.7679, B=12.6262</p> <p>QAM64 5/6: A=-4.299, B=22.1596</p>

Figure 4.3.5: PER vs. Capacity scattering diagrams for 1x4 SIMO system operating in 1st group of channels in presence of co-channel interferenceFigure 4.3.6: PER vs. MI scattering diagrams for 1x4 SIMO system operating in 1st group of channels in presence of co-channel interference

It can be seen that for SIMO system with 1 Tx and 4 Rx antennas operating in the first group of channels in the presence of co-channel interference the falloffs of the scattering diagrams are still well approximated with log-linear dependence for both Capacity and MI CQIs. The presence of the co-channel interference *does not produce* substantial increase of the deviation of the points of scattering diagrams from approximating curves in comparison with interference-free environment. PHY abstraction model parameters for each modulation and coding scheme are also similar for SIMO operating in interference and interference-free environments.

4.3.2 2nd group of channels

4.3.2.1 SISO

Table 4.3.4: Scattering diagrams and log-linear approximations thereof for SISO system operating in 2nd group of channels

	<p>Parameters of log-linear approximation ($\log_{10}(y)=Ax+B$):</p> <p>QPSK 1/2: $A=-6.8256$, $B=8.1379$</p> <p>QAM16 1/2: $A=-4.5051$, $B=10.7298$</p> <p>QAM64 1/2: $A=-3.7953$, $B=13.8948$</p> <p>QAM64 5/6: $A=-0.89867$, $B=4.7148$</p>
	<p>QPSK 1/2: $A=-12.1818$, $B=13.3648$</p> <p>QAM16 1/2: $A=-5.93$, $B=13.066$</p> <p>QAM64 1/2: $A=-4.0134$, $B=13.4925$</p> <p>QAM64 5/6: $A=-2.2417$, $B=11.012$</p>

For SISO system operating in the second group of channels the falloffs of the scattering diagrams are well approximated with log-linear dependence for both Capacity and MI CQIs. However, it is seen that due to greater frequency selectivity of this group of channels in comparison with the first group the deviation of the points of scattering diagram from the approximating curves for high-order modulations (e.g. QAM64 with code rate 5/6) is substantial. It is also seen that the said deviation for the MI is much less than for the Capacity CQI, though certain outbreaks taking place do not allow for accurate approximation. For lower order modulations it is seen that the parameters of the PHY abstraction models are very close to ones for the same modulation and coding schemes for the first channel model.

4.3.2.2 SIMO 1x4 with MRC at the receiver

Table 4.3.5: Scattering diagrams and log-linear approximations thereof for 1x4 SIMO system operating in 2nd group of channels

	<p>Parameters of log-linear approximation ($\log_{10}(y)=Ax+B$):</p> <p>QPSK 1/2: A=-9.052, B=10.5079</p> <p>QAM16 1/2: A=-5.5766, B=13.208</p> <p>QAM64 1/2: A=-4.0689, B=15.0145</p> <p>QAM64 5/6: A=-3.005, B=16.9196</p>
<p>Figure 4.3.9: PER vs. Capacity scattering diagrams for 1x4 SIMO system operating in 2nd group of channels</p>	<p>QPSK 1/2: A=-11.2762, B=12.4442</p> <p>QAM16 1/2: A=-6.1105, B=13.5511</p> <p>QAM64 1/2: A=-4.1448, B=14.0677</p> <p>QAM64 5/6: A=-4.707, B=24.3041</p>
	<p>QPSK 1/2: A=-11.2762, B=12.4442</p> <p>QAM16 1/2: A=-6.1105, B=13.5511</p> <p>QAM64 1/2: A=-4.1448, B=14.0677</p> <p>QAM64 5/6: A=-4.707, B=24.3041</p>
<p>Figure 4.3.10: PER vs. MI scattering diagrams for 1x4 SIMO system operating in 2nd group of channels</p>	

It can be seen that for SIMO system with 1 Tx and 4 Rx antennas operating in the second group of channels the falloffs of the scattering diagrams are well approximated with log-linear dependence for both Capacity and MI CQIs. Since the effective channel transfer function after removing the spatial diversity is much flatter than for SISO system, the deviation of the points of scattering diagrams from approximating curves is even smaller than for SISO system operating in the same channel. Comparing PHY abstraction model parameters of each modulation and coding scheme, one can note that they are similar for SIMO and SISO systems. The similarity of parameters also takes place for SIMO system operating in the first and in the second group of channels.

4.3.2.3 SIMO 1x4 with MMSE receiver in presence of co-channel interference

Table 4.3.6: Scattering diagrams and log-linear approximations thereof for 1x4 SIMO system operating in 2nd group of channels in presence of co-channel interference

	<p>Parameters of log-linear approximation ($\log_{10}(y)=Ax+B$):</p> <p>QPSK 1/2: A=-8.7684, B=10.0954</p> <p>QAM16 1/2: A=-5.6073, B=13.2949</p> <p>QAM64 1/2: A=-3.9418, B=14.4653</p> <p>QAM64 5/6: A=-3.0603, B=17.2716</p>
<p>Figure 4.3.11: PER vs. Capacity scattering diagrams for 1x4 SIMO system operating in 2nd group of channels in presence of co-channel interference</p>	<p>QPSK 1/2: A=-10.6922, B=11.7317</p> <p>QAM16 1/2: A=-6.1467, B=13.6365</p> <p>QAM64 1/2: A=-4.0454, B=13.6594</p> <p>QAM64 5/6: A=-4.558, B=23.5082</p>
<p>Figure 4.3.12: PER vs. MI scattering diagrams for 1x4 SIMO system operating in 2nd group of channels in presence of co-channel interference</p>	

It can be seen that for SIMO system with 1 Tx and 4 Rx antennas operating in the second group of channels in the presence of co-channel interference the falloffs of the scattering diagrams are still well approximated with log-linear dependence for both Capacity and MI CQIs. In this group of channels *the presence of the frequency-selective co-channel interference leads to noticeable increase of the deviation of the points of scattering diagrams from approximating curves for high-order modulation for Capacity CQI, while the MI-based models show greater robustness in terms of this deviation.* PHY abstraction model parameters for each modulation and coding scheme are also similar for SIMO operating in interference and interference-free environments, though increased deviation limits the accuracy of the approximation for high-order modulation.

4.3.2.4 Alamouti scheme 2x4

Table 4.3.7: Scattering diagrams and log-linear approximations thereof for Alamouti scheme with 2 transmit and 4 receive antennas operating in 2nd group of channels

	<p>Parameters of log-linear approximation ($\log_{10}(y)=Ax+B$):</p> <p>QPSK 1/2: A=-8.7773, B=10.0639</p> <p>QAM16 1/2: A=-5.3116, B=12.4926</p> <p>QAM64 1/2: A=-3.4597, B=12.5879</p> <p>QAM64 5/6: A=-2.9327, B=16.4157</p>
<p>Figure 4.3.13: PER vs. Capacity scattering diagrams for Alamouti scheme with 2 transmit and 4 receive antennas operating in 2nd group of channels</p>	<p>QPSK 1/2: A=-10.8557, B=11.921</p> <p>QAM16 1/2: A=-5.8069, B=12.7985</p> <p>QAM64 1/2: A=-3.5185, B=11.7679</p> <p>QAM64 5/6: A=-4.3006, B=22.1503</p>
<p>Figure 4.3.14: PER vs. MI scattering diagrams for Alamouti scheme with 2 transmit and 4 receive antennas operating in 2nd group of channels</p>	

The falloffs of the scattering diagrams for the system using STC-A (Alamouti) scheme with 2 Tx and 4 Rx antennas in the second group of channels are well approximated with the log-linear dependence with the negligible deviation of points of the diagram from the approximating curve. The parameters of the PHY abstraction models are similar to ones of the models for other multi-antenna techniques and channel models. Since this mode of operation in this channel shows the smallest deviation from the approximating curves for both Capacity and MI based CQIs, *the parameters of this PHY abstraction model are taken as etalon and are used for validation of the developed PHY abstraction methodology performed in the Paragraph 4.5.*

4.3.2.5 Spatial multiplexing scheme 2x4

Table 4.3.8: Scattering diagrams and log-linear approximations thereof for Spatial Multiplexing scheme with 2 transmit and 4 receive antennas operating in 2nd group of channels

	<p>Parameters of log-linear approximation ($\log_{10}(y)=Ax+B$):</p> <p>QPSK 1/2: A=-4.8289, B=5.2136</p> <p>QAM16 1/2: A=-3.4807, B=7.9944</p> <p>QAM64 1/2: A=-2.8982, B=10.4464</p> <p>QAM64 5/6: A=-1.8305, B=10.2883</p>
<p>Figure 4.3.15: PER vs. Capacity scattering diagrams for Spatial Multiplexing scheme with 2 transmit and 4 receive antennas operating in 2nd group of channels</p>	<p>QPSK 1/2: A=-6.3969, B=6.6385</p> <p>QAM16 1/2: A=-3.9069, B=8.3568</p> <p>QAM64 1/2: A=-3.016, B=9.9804</p> <p>QAM64 5/6: A=-4.3249, B=22.275</p>
<p>Figure 4.3.16: PER vs. MI scattering diagrams for Spatial Multiplexing scheme with 2 transmit and 4 receive antennas operating in 2nd group of channels</p>	

It can be seen that the falloffs of the scattering diagrams for the system using STC-B (spatial multiplexing) scheme with 2 Tx and 4 Rx antennas in the second group of channels are well approximated with the log-linear dependence. However, the deviation of points of the diagram from the approximating curve increases in comparison with STC-A mode; the deviation for Capacity-based CQU being greater than for MI-based CQI. The increase of the deviation leads to the fact that the parameters of the PHY abstraction models differ from ones of other multi-antenna techniques and channel models (e.g. STC-A of the second group of channels). However, we believe that this does not mean that this mode of operation requires special parameters of PHY abstraction model, and results of validation presented in the following paragraphs confirm this point of view.

4.3.3 3rd group of channels

4.3.3.1 SISO

Table 4.3.9: Scattering diagrams and log-linear approximations thereof for SISO system operating in 3rd group of channels

	<p>Parameters of log-linear approximation ($\log_{10}(y)=Ax+B$):</p> <p>QPSK 1/2: $A=-6.3524$, $B=7.2479$</p> <p>QAM16 1/2: $A=-4.8426$, $B=11.4474$</p> <p>QAM64 1/2: $A=-3.6428$, $B=13.2758$</p> <p>QAM64 5/6: $A=-1.3055$, $B=6.9959$</p>
	<p>QPSK 1/2: $A=-11.729$, $B=12.8846$</p> <p>QAM16 1/2: $A=-5.8019$, $B=12.8142$</p> <p>QAM64 1/2: $A=-3.9248$, $B=13.1625$</p> <p>QAM64 5/6: $A=-4.4023$, $B=22.6043$</p>

Figure 4.3.17: PER vs. Capacity scattering diagrams for SISO system operating in 3rd group of channels

Figure 4.3.18: PER vs. MI scattering diagrams for SISO system operating in 3rd group of channels

The falloffs of the scattering diagrams for the SISO system operating in the third group of channels are well approximated with the log-linear dependence for both Capacity based and MI based CQIs. *Substantial frequency selectivity of the channel of the third group leads to considerable deviation of the points of the scattering diagrams from the approximating curves for high order modulation.* It can be also seen that MI-based CQI provides much less deviation than Capacity-based. The parameters of the resulting PHY abstraction models are similar to ones measured for other channel models and multi-antenna techniques. This is especially true for the MI-based CQI.

4.3.3.2 SIMO 1x4 with MRC at the receiver

Table 4.3.10: Scattering diagrams and log-linear approximations thereof for 1x4 SIMO system operating in 3rd group of channels

	<p>Parameters of log-linear approximation ($\log_{10}(y)=Ax+B$):</p> <p>QPSK 1/2: A=-9.4348, B=11.0496</p> <p>QAM16 1/2: A=-5.0203, B=11.7943</p> <p>QAM64 1/2: A=-3.8736, B=14.184</p> <p>QAM64 5/6: A=-2.0763, B=11.392</p>
<p>Figure 4.3.19: PER vs. Capacity scattering diagrams for 1x4 SIMO system operating in 3rd group of channels</p>	<p>QPSK 1/2: A=-11.5839, B=12.8007</p> <p>QAM16 1/2: A=-5.5221, B=12.1425</p> <p>QAM64 1/2: A=-3.9763, B=13.3931</p> <p>QAM64 5/6: A=-4.4078, B=22.681</p>
<p>Figure 4.3.20: PER vs. MI scattering diagrams for 1x4 SIMO system operating in 3rd group of channels</p>	

It can be seen that the falloffs of the scattering diagrams for the SIMO system with 4 Rx antennas operating in the third group of channels are well approximated with the log-linear dependence for both Capacity based and MI based CQIs. Frequency selectivity of the channel of the third group is substantially reduced after removing the spatial diversity by applying MRC at the receiver side. This results in less deviation of the points of the scattering diagrams from the approximating curves in comparison with the SISO system. As a consequence, the parameters of the PHY abstraction models are similar to ones measured for other channels and multi-antenna techniques.

4.3.3.3 Alamouti scheme 2x4

Table 4.3.11: Scattering diagrams and log-linear approximations thereof for Alamouti scheme with 2 transmit and 4 receive antennas operating in 3rd group of channels

	<p>Parameters of log-linear approximation ($\log_{10}(y)=Ax+B$):</p> <p>QPSK 1/2: A=-8.782, B=10.0743</p> <p>QAM16 1/2: A=-5.1377, B=12.0316</p> <p>QAM64 1/2: A=-3.9585, B=14.5048</p> <p>QAM64 5/6: A=-2.8767, B=16.0223</p>
<p>Figure 4.3.21: PER vs. Capacity scattering diagrams for Alamouti scheme with 2 transmit and 4 receive antennas operating in 3rd group of channels</p>	<p>QPSK 1/2: A=-11.2091, B=12.3527</p> <p>QAM16 1/2: A=-5.5916, B=12.2755</p> <p>QAM64 1/2: A=-4.0268, B=13.5708</p> <p>QAM64 5/6: A=-4.3754, B=22.5158</p>
	<p>Figure 4.3.22: PER vs. MI scattering diagrams for Alamouti scheme with 2 transmit and 4 receive antennas operating in 3rd group of channels</p>

The falloffs of the scattering diagrams for the system using STC-A (Alamouti) scheme with 2 Tx and 4 Rx antennas in the third group of channels are well approximated with the log-linear dependence with only a small deviation of points of the diagram from the approximating curve. The parameters of the PHY abstraction models are similar to ones of the models for other multi-antenna techniques and channels.

4.4 Conclusions on simulation results

Table 4.4.1 summarizes the parameters of log-linear approximation for PHY abstraction models of all measured modes of operation for selected modulation and coding schemes (MCS). It is seen that corresponding parameters do not significantly depend on the group of channels the system operates in or the multi-antenna signal processing technique involved. For example A and B parameters for QAM64 with code rate 5/6 are equal to -4.6 and 23.5 respectively for 1x4 SIMO system operating in the second group of channels, and the same parameters are equal to -4.4 and 22.5 respectively for 2x4 STC-A system operating in third group of channels.

It is also seen that the system and channel pair having approximation coefficients outstanding from the common intervals have substantial deviation of points of the scattering diagrams, and therefore corresponding coefficients cannot be considered measured accurately enough.

Therefore we conclude that one may use parameters of PHY abstraction model measured for the system having particular antenna configuration operating in a particular channel and exploiting particular signal processing technique to predict the performance of the system with any antenna configuration and operating in any of the MEMBRANE channels. In this regard, it is preferable to take the system having the smallest deviation of the points of scattering diagram from the approximation curves as the etalon, i.e. the system providing the best accuracy of the approximation. For generating the PHY abstraction model parameters for this deliverable we have chosen the system with 2 Tx and 2Rx antennas using the STC-A (Alamouti) scheme at the transmitter and linear MMSE MIMO detector at the receiver (highlighted in the Table 4.4.1).

Table 4.4.1: Parameters of log-linear approximation for PHY abstraction models ($\log_{10}(y)=Ax+B$)

Channel/Antenna configuration	MCS	A (Capacity)	B (Capacity)	A (Mutual Information)	B (Mutual Information)
1 st group of channels / SISO	QPSK 1/2	-7.9	9.1	-10.8	11.9
	QAM16 1/2	-5.9	14.1	-6.6	14.6
	QAM64 1/2	-3.8	13.7	-3.8	12.8
	QAM64 5/6	-2.9	16.4	-4.4	22.9
1 st group of channels / SIMO 1x4	QPSK 1/2	-8.9	10.2	-10.6	11.6
	QAM16 1/2	-5.5	13.0	-5.9	13.0
	QAM64 1/2	-3.9	14.3	-4.0	13.5
	QAM64 5/6	-3.0	16.7	-4.2	21.8
1 st group of channels / SIMO 1x4 with CCI	QPSK 1/2	-9.5	11.0	-11.4	12.6
	QAM16 1/2	-5.1	11.8	-5.4	11.8
	QAM64 1/2	-3.7	13.3	-3.8	12.6
	QAM64 5/6	-3.0	16.9	-4.3	22.2
2 nd group of channels / SISO	QPSK 1/2	-6.8	8.1	-12.2	13.4
	QAM16 1/2	-4.5	10.7	-5.9	13.1
	QAM64 1/2	-3.8	13.9	-4.0	13.5
	QAM64 5/6	-0.9	4.7	-2.2	11.0
2 nd group of channels / SIMO 1x4	QPSK 1/2	-9.1	10.5	-11.3	12.4
	QAM16 1/2	-5.6	13.2	-6.1	13.6
	QAM64 1/2	-4.1	15.0	-4.1	14.1

	QAM64 5/6	-3.0	16.9	-4.7	24.3
2 nd group of channels / SIMO 1x4 with CCI	QPSK 1/2	-8.8	10.1	-10.7	11.7
	QAM16 1/2	-5.6	13.3	-6.1	13.6
	QAM64 1/2	-3.9	14.5	-4.0	13.7
	QAM64 5/6	-3.1	17.3	-4.6	23.5
2 nd group of channels / STC-A 2x4	QPSK 1/2	-8.8	10.1	-10.9	11.9
	QAM16 1/2	-5.3	12.5	-5.8	12.8
	QAM64 1/2	-3.5	12.6	-3.5	11.8
	QAM64 5/6	-2.9	16.4	-4.3	22.2
2 nd group of channels / STC-B 2x4	QPSK 1/2	-4.8	5.2	-6.4	6.6
	QAM16 1/2	-3.5	8.0	-3.9	8.4
	QAM64 1/2	-2.9	10.4	-3.0	10.0
	QAM64 5/6	-1.8	10.3	-4.3	22.3
3 rd group of channels / SISO	QPSK 1/2	-6.4	7.2	-11.7	12.9
	QAM16 1/2	-4.8	11.4	-5.8	12.8
	QAM64 1/2	-3.6	13.3	-3.9	13.2
	QAM64 5/6	-1.3	7.0	-4.4	22.6
3 rd group of channels / SIMO 1x4	QPSK 1/2	-9.4	11.0	-11.6	12.8
	QAM16 1/2	-5.0	11.8	-5.5	12.1
	QAM64 1/2	-3.9	14.2	-4.0	13.4
	QAM64 5/6	-2.1	11.4	-4.4	22.7
3 rd group of channels / STC-A 2x4	QPSK 1/2	-8.9	10.1	-11.2	12.4
	QAM16 1/2	-5.1	12.0	-5.6	12.3
	QAM64 1/2	-4.0	14.5	-4.0	13.6
	QAM64 5/6	-2.9	16.0	-4.4	22.5

4.5 Validation of the PHY abstraction methodology

This section investigates the PHY layer performance prediction ability of the developed PHY abstraction model. The average PER performance vs. average SNR curves are used as indicators, where average is taken over multiple channel realizations. To check the accuracy of the performance prediction we plot both the directly measured and the predicted performance curves and estimate the difference between them. Comparison is performed for two channel quality indicators namely Mean Instantaneous Capacity within the FEC block and Mean Mutual Information within the FEC block. For the sake of reducing computational efforts only a representative subset of all available modulation and coding schemes is used to investigate the prediction accuracy. This subset includes the most robust schemes (QPSK with code rate 1/2) for which accuracy of prediction is expected to be the highest as well as the least robust scheme (QPSK-64 with code rate 5/6) which is expected to have the lowest accuracy of performance prediction. Therefore the subset provides good representation of prediction accuracy for all modulation and coding schemes.

For reasons given in the foregoing paragraph, the parameters of the PHY abstraction models used for prediction the PHY layer performance were taken as measured for Alamouti scheme with two transmit and four receive antennas operating in the channel model of second group of channels.

4.5.1 1st group of channels

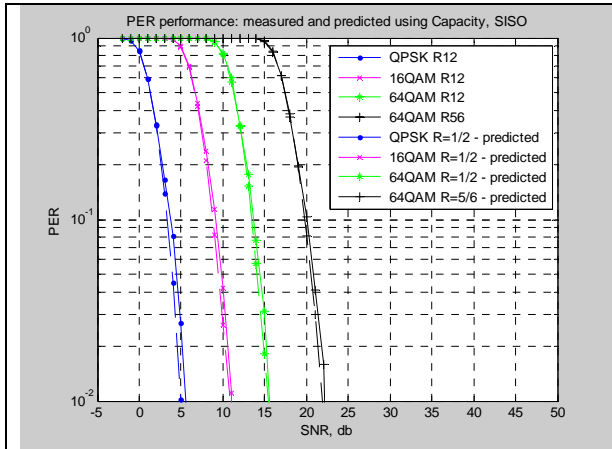


Figure 4.5.1: Capacity-based PHY abstraction prediction accuracy for SISO system operating in 1st group of channels

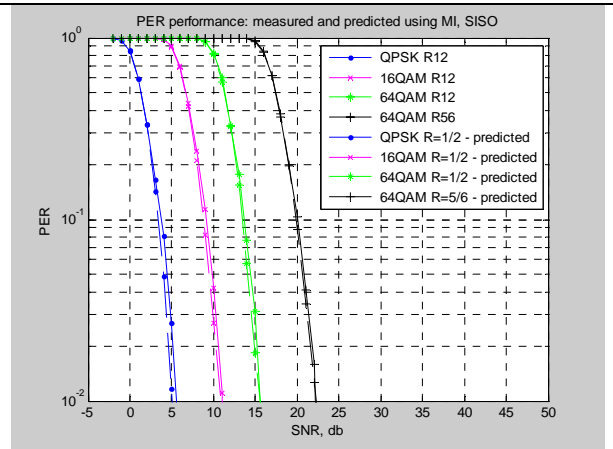


Figure 4.5.2: MI-based PHY abstraction prediction accuracy for SISO system operating in 1st group of channels

It can be seen that for the SISO system operating in the first group of channels the accuracy of the average BLER prediction is very good. Equivalent SNR error of the prediction is less than 1 dB.

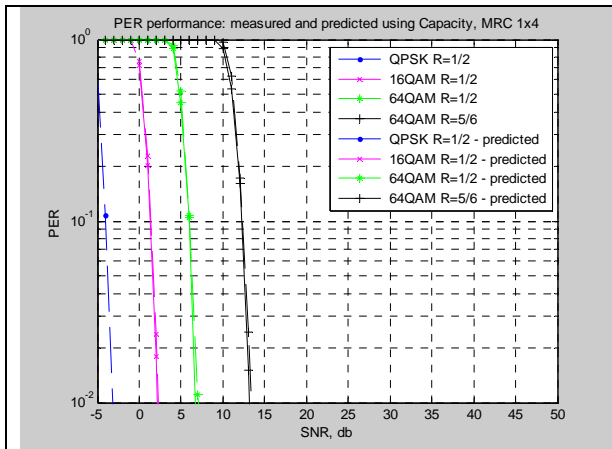


Figure 4.5.3: Capacity based PHY abstraction prediction accuracy for 1x4 SIMO system operating in 1st group of channels

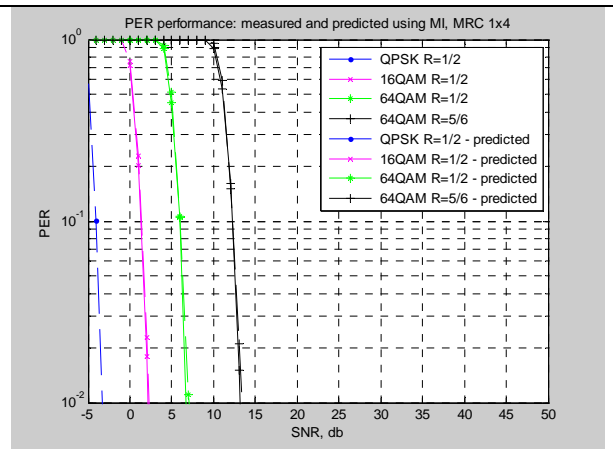


Figure 4.5.4: MI based PHY abstraction prediction accuracy for 1x4 SIMO system operating in 1st group of channels

It is seen that for 1x4 SIMO system operating in the first group of channels the error of average BLER prediction is almost negligible.

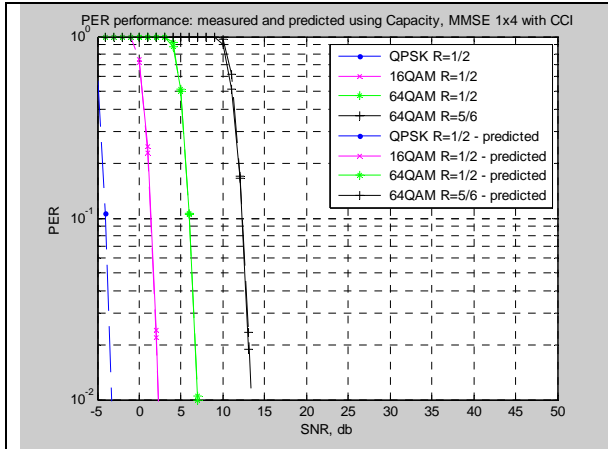


Figure 4.5.5: Capacity based PHY abstraction prediction accuracy for 1x4 SIMO system operating in 1st group of channels in presence of co-channel interference

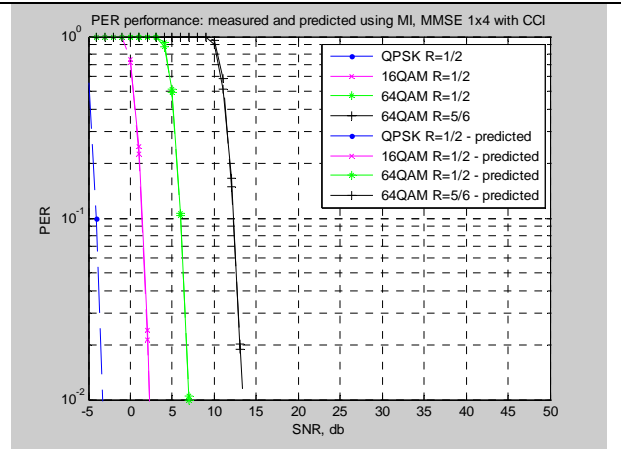


Figure 4.5.6: MI based PHY abstraction prediction accuracy for 1x4 SIMO system operating in 1st group of channels in presence of co-channel interference

It is seen that presence of a single co-channel interferer on the direction of 30 degrees with respect to the link between the two nodes does not affect the accuracy of BLER prediction for the 1x4 SIMO system operating in the first group of channels.

4.5.2 2nd group of channels

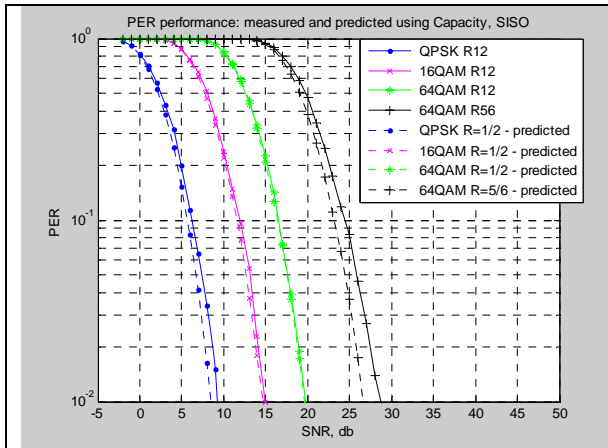


Figure 4.5.7: Capacity based PHY abstraction prediction accuracy for SISO system operating in 2nd group of channels

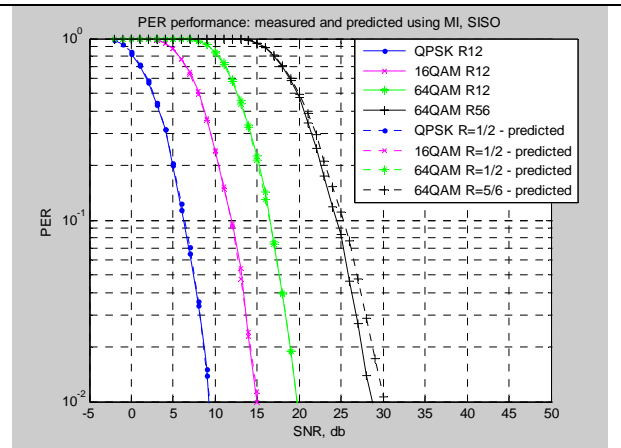


Figure 4.5.8: MI based PHY abstraction prediction accuracy for SISO system operating in 2nd group of channels

It is seen that for the SISO system operating in the second group of channels the error of BLER prediction is considerable. For example, for the Capacity-based CQI the equivalent SNR error may achieve 1.5-2 dB for high order modulation. It is also seen that the Capacity-based CQI provides optimistic estimate of the system BLER performance, whereas the MI-based CQI provides accurate prediction for the most of MCSs, and only for the highest-order modulation it gives pessimistic estimate.

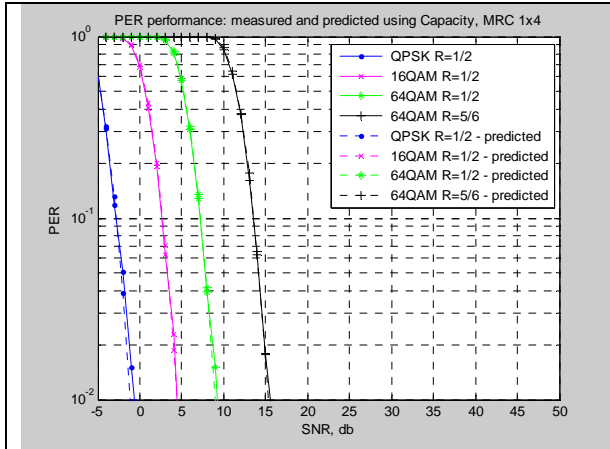


Figure 4.5.9: Capacity based PHY abstraction prediction accuracy for 1x4 SMIO system operating in 2nd group of channels

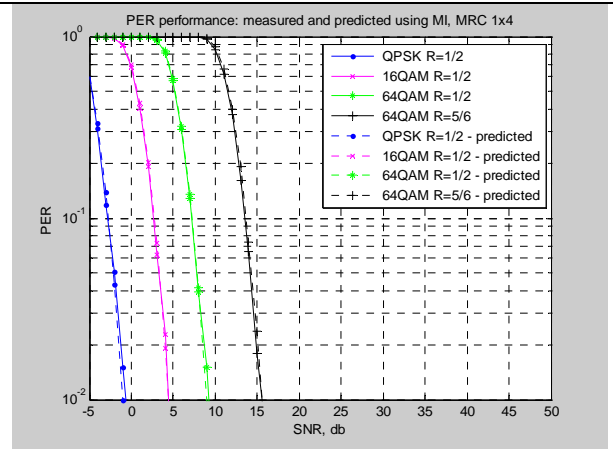


Figure 4.5.10: MI based PHY abstraction prediction accuracy for 1x4 SMIO system operating in 2nd group of channels

For 1x4 SIMO system operating in the second group of channels the accuracy of BLER prediction is very good for both CQIs.

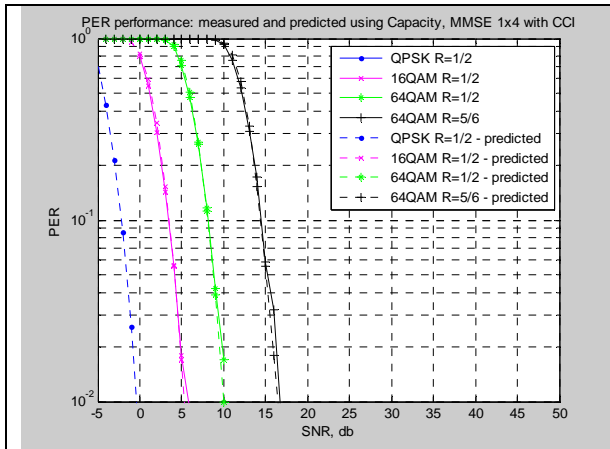


Figure 4.5.11: Capacity based PHY abstraction prediction accuracy for 1x4 SMIO system operating in 2nd group of channels in presence of co-channel interference

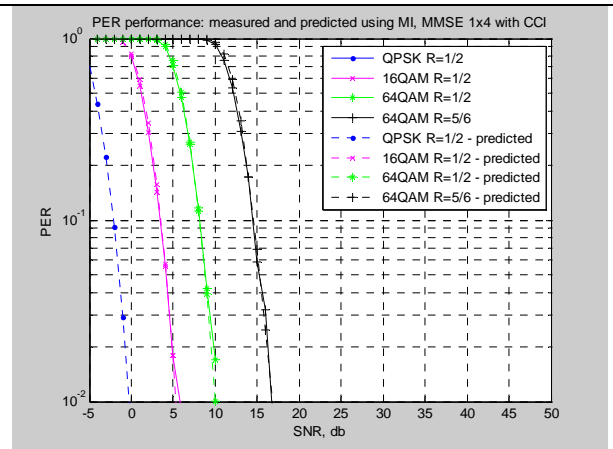


Figure 4.5.12: MI based PHY abstraction prediction accuracy for 1x4 SMIO system operating in 2nd group of channels in presence of co-channel interference

It is seen that presence of a single co-channel interferer on the direction of 30 degrees with respect to the link between the two nodes does not affect the accuracy of BLER prediction for the 1x4 SIMO system operating in the second group of channels.

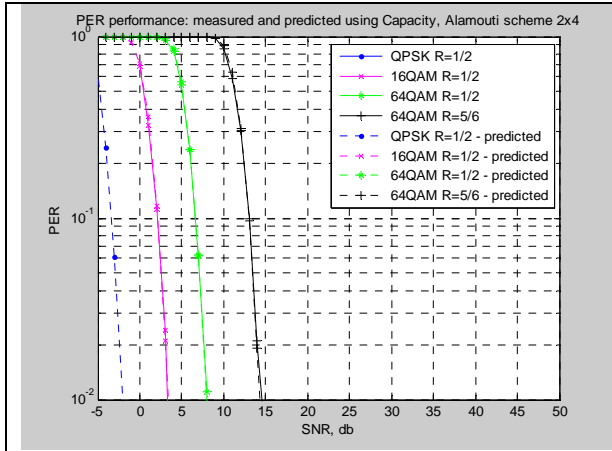


Figure 4.5.13: Capacity based PHY abstraction prediction accuracy for Alamouti scheme with 2 transmit 4 receive antennas operating in 2nd group of channels

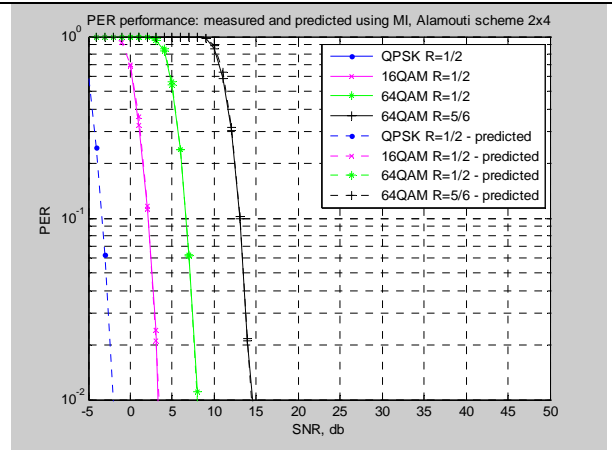


Figure 4.5.14: MI based PHY abstraction prediction accuracy for Alamouti scheme with 2 transmit 4 receive antennas operating in 2nd group of channels

It can be seen that the error of BLER prediction for 2x4 system operating in the second group of channels and using STC-A (Alamouti) scheme at the transmitter and linear MMSE MIMO detector at the receiver is negligible.

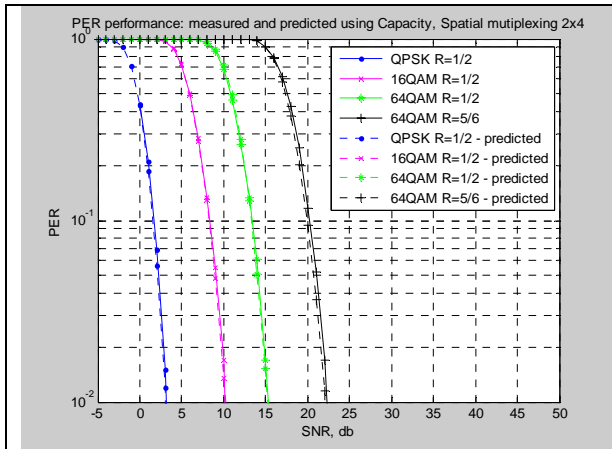


Figure 4.5.15: Capacity based PHY abstraction prediction accuracy for Spatial Multiplexing scheme with 2 transmit 4 receive antennas operating in 2nd group of channels

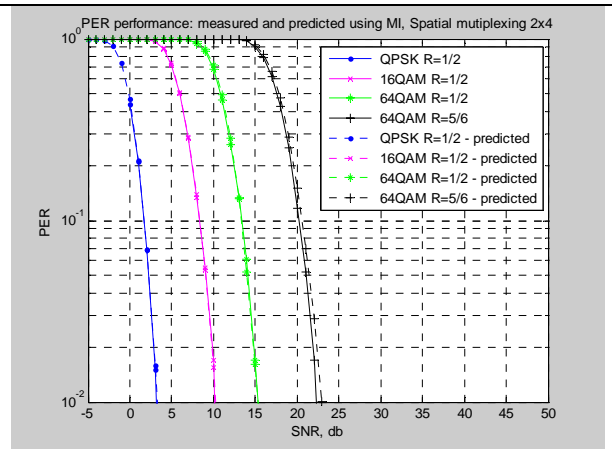


Figure 4.5.16: MI based PHY abstraction prediction accuracy for Spatial Multiplexing scheme with 2 transmit 4 receive antennas operating in 2nd group of channels

It can be seen that the accuracy of BLER prediction for 2x4 system operating in the second group of channels and using STC-B (spatial multiplexing) scheme at the transmitter and linear MMSE MIMO detector at the receiver is very good. The equivalent SNR error of prediction is within 1 dB for both CQIs. It is also seen that the estimate produced using the Capacity-based CQI tends to be optimistic, whereas MI-based CQI gives more precise estimate that tends to be pessimistic.

4.5.3 3rd group of channels

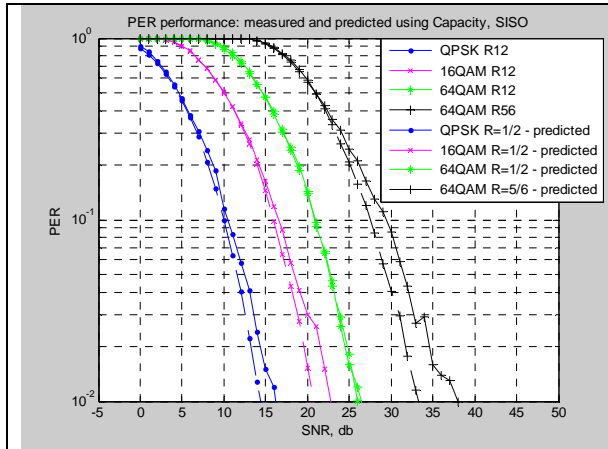


Figure 4.5.17: Capacity based PHY abstraction prediction accuracy for SISO system operating in 3rd group of channels

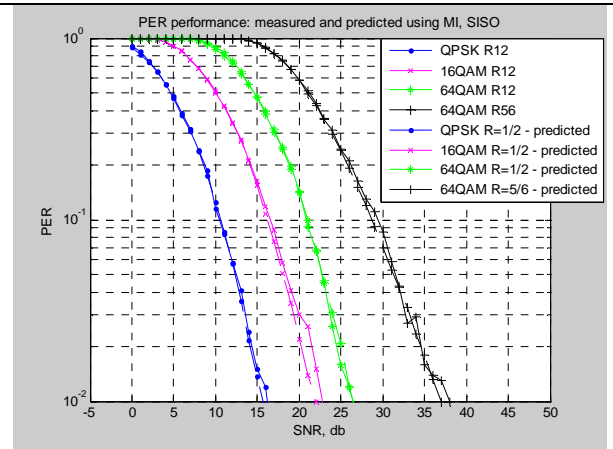


Figure 4.5.18: MI based PHY abstraction prediction accuracy for SISO system operating in 3rd group of channels

It is seen that greater frequency selectivity and variability of the channel of the third group leads to substantial error of BLER prediction for SISO system operating in that channel. It is also seen that using the Capacity-based CQI leads to optimistic estimate of the BLER performance of the system, whereas the estimate obtained with the help of the MI is close to directly-measured performance. Besides, using the MI-based CQI gives much more accurate estimate. The equivalent SNR error of the estimate is within 1.5 dB for MI-based CQI and is up to 3dB for the Capacity-based CQI.

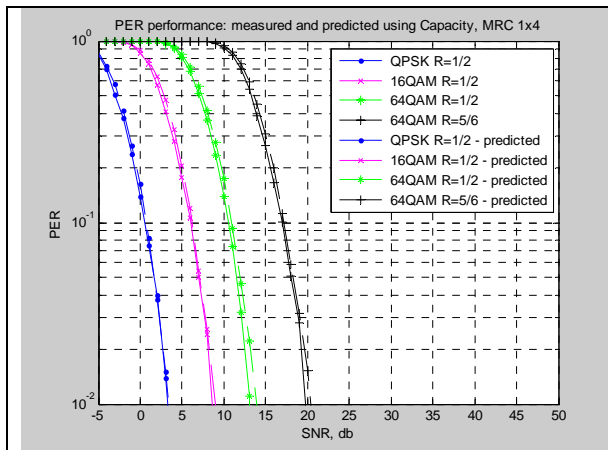


Figure 4.5.19: Capacity based PHY abstraction prediction accuracy for 1x4 SMIO system operating in 3rd group of channels

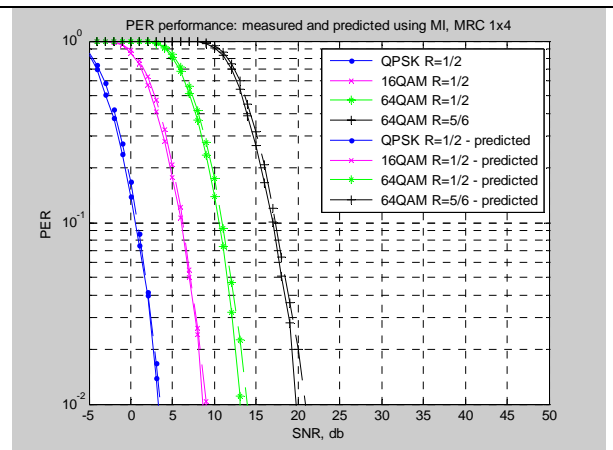


Figure 4.5.20: MI based PHY abstraction prediction accuracy for 1x4 SMIO system operating in 3rd group of channels

It is seen that for 1x4 SIMO system the accuracy BLER prediction is very good even for that frequency-selective and variable channel as one of the third group. Eh equivalent SNR error of BLER prediction is within 1 dB for both CQIs.

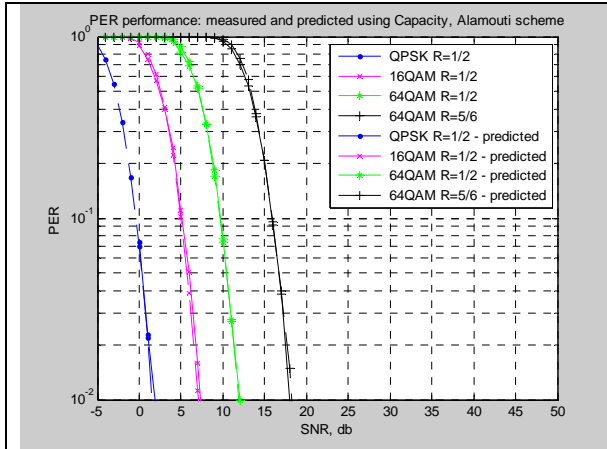


Figure 4.5.21: Capacity based PHY abstraction prediction accuracy for Alamouti scheme with 2 transmit 4 receive antennas operating in 3rd group of channels

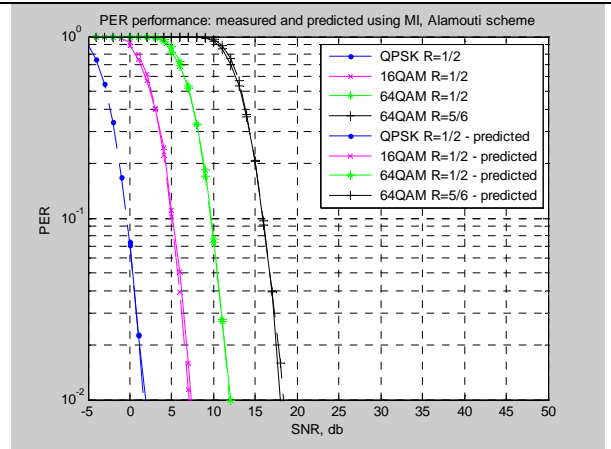


Figure 4.5.22: MI based PHY abstraction prediction accuracy for Alamouti scheme with 2 transmit 4 receive antennas operating in 3rd group of channels

It can be seen that the error of BLER prediction for 2x4 system operating in the third group of channels and using STC-A (Alamouti) scheme at the transmitter and linear MMSE MIMO detector at the receiver is almost negligible.

4.6 Summary on the PHY abstraction methodology validation

Upon the results of the PHY abstraction methodology presented in the foregoing paragraph, the following conclusions can be drawn.

It is seen that the PHY abstraction model with parameters measured for particular etalon system provides good prediction accuracy for the whole range of systems operating in different channel models.

The prediction accuracy of the MI-based PHY abstraction model is in general better than Capacity-based model. This is mainly explained by the slightly different nature of the two CQIs. The Capacity provides the estimate of the maximum achievable amount of information that can be transmitted through a channel assuming ideally chosen modulation order and coding type/rate from the infinite set thereof. On the other hand, MI gives the estimate of the achievable amount of information that can be transmitted through a channel taking into account the particular modulation order.

The PHY abstraction model based on the mean instantaneous capacity within the FEC block as a CQI tends to provide optimistic estimate of the link error performance. This is also explained by the nature of the Capacity as a CQI. For some good channel realizations having substantial channel gain the Capacity indicates that big information amount may be sent through the channel. However, the real information amount is also limited by the maximum modulation order used in the system.

With the increase of the number of receive antennas, the accuracy of prediction of the PHY layer performance generally increases. This is explained by the fact that using bigger number of antennas substantially reduces the frequency selectivity of the channel, which leads to higher correlation between the CQI and the LQI.

5 CONCLUSIONS

In this report we have developed the PHY abstraction methodology essential for performance evaluation of the OFDMA-based communication systems with the help of system-level simulations. The proposed methodology allows dramatically reducing the amount of computations needed to estimate the error probabilities of signal transmissions being sent through a channel with given characteristics using predetermined multi-antenna techniques.

The developed PHY abstraction methodology is based on log-linear approximation of the pre-measured dependence between the channel quality indicator and the link quality indicator. Two channel quality indicators, namely the Mean Instantaneous Capacity within the FEC block and the Mean Mutual Information within the FEC block were considered. FEC coding block error ratio (BLER) was used as a link quality indicator.

In this report we present the exact ready-to-use parameters of the developed PHY abstraction models derived with the help of the link-level simulator developed in the [MEM D511]. We show that the parameters of the PHY abstraction models do not depend significantly on the channel models or the multi-antenna techniques employed. Therefore the whole range of techniques typically used to improve the link robustness to noise and interference, or to adapt the transmissions to the channel and interference environment can be described with the single set of parameters.

Overall, the report contains the detailed description and exact parameters of the physical layer abstraction models applicable for all possible link types of MEMBRANE network. The models presented in this report will be directly used to predict the PHY layer performance of individual links in the system-level simulations of the work-package WP5.1.

TERMS AND ACRONYMS

AMC	Advanced modulation and coding
AoA	Angle of arrival
AoD	Angle of departure
CCI	Co-channel interference
CDL	Clustered delay line
CQI	Channel quality indicator
CTC	Convolutional turbo-code
DL	Downlink
LLS	Link-level simulations/simulator
LOS	Line-of-sight
LQI	Link quality indicator
MAC	Medium access control
MF	Matched filter
MI	Mutual information
MIMO	Multiple-input-multiple-output
MMSE	Minimum mean-square error
MRC	Maximum-ratio combining
NLOS	Non-line-of sight
OC	Optimal combining
OFDM	Orthogonal frequency-division multiplexing
OFDMA	Orthogonal frequency-division multiple access
PHY	Physical layer
PUSC	Partial usage of subchannels
QAM	Quadrature-amplitude modulation
QPSK	Quadrature phase-shift keying
RRM	Radio resource management
SCM	Spatial channel model
SDMA	Space-division multiple access
SIMO	Single-input-multiple-output
SISO	Single-input-single-output
SINR	Signal-to-interference-plus-noise ratio
SIR	Signal-to-interference ratio
SLS	System-level simulations/simulator
SM	Spatial multiplexing
SNR	Signal-to-noise ratio

STC	Space-time coding
UL	Uplink
ZF	Zero-forcing

REFERENCES

- [16j-06/020] IEEE C802.16j-06/020, "Channel Models and Performance Metrics for IEEE 802.16j Relay Task Group", May 1, 2006
- [802.16] IEEE 802.16e-2005
- [Alamouti] S. M. Alamouti, "Simple Transmit Diversity Technique for Wireless Communications," IEEE Journal on Select Areas in Communications, vol.16, pp. 1451-1458, 1998.
- [Caire] Caire G., Taricco G., and Biglieri E., "Capacity of bit-interleaved channels," Electronic Letters, vol. 32, no. 12, pp 1060-1061, June 1996.
- [Dent et al] Dent, P.; Bottomley, G.E.; Croft, T. "Jakes fading model revisited" Electronics Letters, Vol. 29 , Issue: 13 , 24 June 1993
- [Erc01] V. Erceg, et al. "TGn channel models" IEEE doc. #11-03-0940-03cl-000n, May 2004
- [Ericsson] Ericsson, "Effective SNR mapping for modeling frame error rates in multiple-state channels," 3GPP2-C30-20030429-010
- [ITU-R M.1225] Recommendation ITU-R M.1225, "Guidelines for Evaluation of Radio Transmission Technologies for IMT-2000"
- [Li, Huang] Y. Li and X. Huang, "The generation of independent Rayleigh faders," IEEE International Conference on Communications, ICC 2000, vol. 1, pp. 41-45, 2000.
- [MEM D21] IST-MEMBRANE, Deliverable 2.1, "Most relevant community/market needs and target deployment scenarios for wireless backhaul multi-element multihop networks" July, 2006
- [MEM D411] IST-MEMBRANE, Deliverable 4.1.1, "Reconfigurable IA/MIMO Transceiver Algorithms"
- [MEM D511] IST-MEMBRANE, Deliverable 5.1.1, "Comprehensive PHY layer model and performance analysis of the PHY link for different scenarios"
- [Schumacher at al] L. Schumacher, K. I. Pedersen, and P.E. Mogensen, "From antenna spacings to theoretical capacities – guidelines for simulating MIMO systems," in Proc. PIMRC Conf., vol. 2, Sept. 2002, pp. 587-592.
- [SCM] 3GPP & 3GPP2 Spatial Channel Model Ad-Hoc Group, "Spatial Channel Model Text Description. SCM Text V6.0", April 2003
- [WIN D54] WINNER Deliverable D5.4, V1.4, "Final report on link level and system level channel models", November 2005, <https://www.ist-winner.org/>
- [Winters] J. H. Winters, "Optimum combining in digital mobile radio with co-channel interference", IEEE Trans. Vehicular Technol. 33(3) (1984) 144-155.
- [Zha04] G. Zhao and S. Loyka, "Impact of multipath clustering on the performance of MIMO Systems," in Proc. of IEEE Wireless Communication and Networking Conf. (WCNC), Atlanta, Georgia, USA, March 2004.
- [Zhang, Li] Y. Zhang; D. Li, "MMSE linear detector for space-time transmit diversity over fast fading channels", Personal, Indoor and Mobile Radio Communications, 2003. PIMRC 2003.